# Visualization of dynamic loading-induced damages of rock-like materials using Micro-focus X-ray CT system

Sang-Ho Cho, Suel-Ki Cho, Seung-KonKim (Chonbuk National University)
Dae-Sung Choen, Jung-Ho Synn (KIGAM)
Kaneko Katsuhiko (Hokkaido University, Japan)

## 1. INTRODUCTION

Damage assessment of rock materials subjected to dynamic loading is very important in fracture control in blasting and underground excavation for nuclear waste disposal with rock and concrete forming a barrier against possible seepage or leaking.

Split Hopkinson Pressure Bar (SHPB) technique has been widely used to investigate the dynamic strength and response of materials in the strain rate up to $10^3$ /s. Based on one-dimensional stress wave analysis, the dynamic strain rate and strain can be calculated (Kolsky 1949; Gray 1999). X-ray computed tomography (CT) was first introduced in the medical field and is now applied for industrial applications (Vineger, 1986). Recently, high-resolution X-ray CT has been used to observe microstructure of mineral particles and rock samples(Lin et al., 1996, Cho et al., 2005)

In this study, pulse shape-controlled Split Hopkinson Pressure Bar system (Nemat-Nasser et al., 1991;Cho et al, 2007) was used to apply a step by step increasing impact to cement paste samples. The impact velocity of impact bar had been increased to 9.8m/sec from 18.67m/sec. The microfocus X-ray Computerized Tomography was used to scan the tested sample. The scanned slices were rendered to build 3D dimensional images of the sample. The damage mechanism of rock-like materials subjected to dynamic loading was discussed.

## 2. MICRO X-RAY COMPUTED TOMOGRAPHY (CT) SYSTEM

The custom designed micro X-ray CT system (TOSCANER 30900μhd), as shown in Fig. 1, which is installed at Hokkaido University, uses multi-scan and cone geometry to observe three-dimensional microstructure of an object. Figure 2 shows a schematic diagram of the micro CT system. X-rays from microfocus X-ray generator are partially attenuated by a specimen that is made to rotate in equal steps in a full circle about a single axis close to its center. At each rotational position, the surviving X-ray photons are detected by an X-ray I.I. (Image Intensifier) large enough to contain the shadow of the

specimen. These projection images are collected using conventional video technology. The video signal is then converted to a two-dimensional digital array by an image processing system. Finally, a three-dimensional image array is reconstructed from the collected set of projection images. The system can achieve 2048×2048 pixel reconstructions and obtain data needed for 3-D image in one scanning session. A high-resolution sensor and enhanced accuracy of image reconstruction software have achieved a spatial resolution of 5μm and finer. In this study the system was used to observe microstructure of the rock specimens before and after a dynamic tensile test.


Fig. 1 High resolution micro X-ray computed tomography (CT) system (TOSCNAR 30900μhd, Toshiba co.)

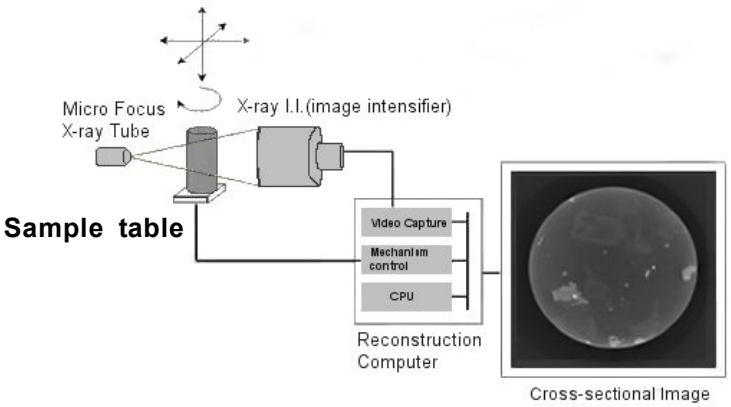


Fig. 2 A schematic diagram of the microfocus X-ray CT system

## 3. DYNAMIC IMPACT TEST AND RESULTS

Figure 3 show a schematic of a suggested Pulse Shape- Controlled SHPB (PSC SHPB) test. SHPB consists of an impact (striker) bar, an incident bar, and a transmission bar. The rock sample is placed between the incident and transmitted bars. A gas gun is used to launch the impact bar. The shape of the incident pulse can be controlled by the gas gun pressure, the length of impact bar, and the dimension

of pulse shaper. We used 27 mm diameter impact, incident (2600 mm length) and transmitted (1600 mm length) bars. The impact velocities of 9.9 m/s- 18 m/s were applied to make dynamic loading-induced damage samples which have different damage levels. The cement mortar sample was used to make test samples. Mechanical properties and geometry of test samples are listed in Table 1. The cylindrical samples were cut and grinded by using precision sample preparing machine. Table 2 shows the summery of the test condition and results from the tests. Apparent strain increased as impact velocity increased while the elastic wave velocity decreased. To avoid separation of the test sample during impact, the samples were wrapped with a flexible tape.

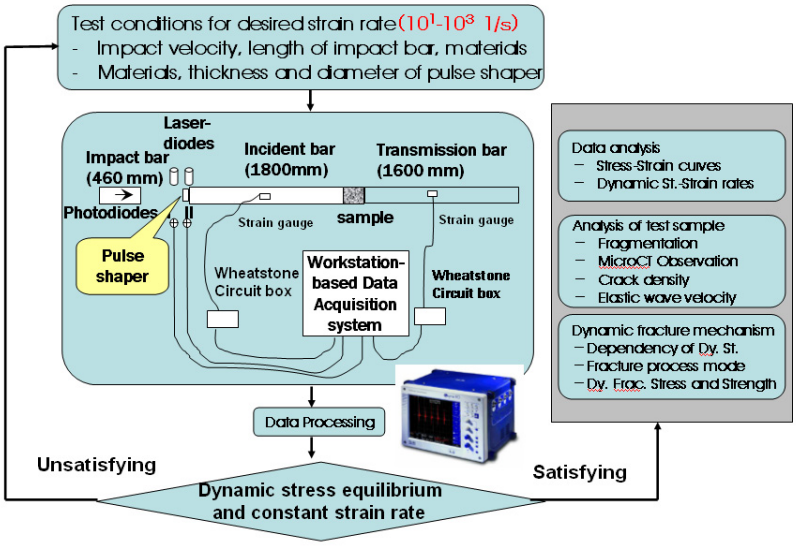


Fig. 3 Flow chart of Pulse-shape Controlled Split Hopkinson Pressure Bar

Table 1. Mechanical properties and geometry of test samples

| No. of Sample | Length (mm) | Diameter (mm) | P-wave Velocity (km/s) | Density (g/cc) |
|---|---|---|---|---|
| B1 | 30 | 31 | 3.5 | 2.2 |
| B2 | 30 | 31 | 3.5 | 2.2 |
| B3 | 30 | 31 | 3.5 | 2.2 |
| B4 | 30 | 31 | 3.5 | 2.2 |

Table 2. Summery of test conditions and the results

| No. of Sample | Gas Pressure (Psi ) | Impact Velocity (m/s) | Ratio of Elastic Wave Velocity before and after Impact | Apparent Strain (%) |
|---|---|---|---|---|
| B1 | 6 | 9.9 | 0.865 | 0 |
| B2 | 10 | 12.4 | 0.593 | 0.07 |
| B3 | 15 | 14.3 | 0.395 | 0.23 |
| B4 | 20 | 18.0 | 0.316 | 0.5 |

## 4. OBSERVATION OF THE TEST SAMPLES USING MICRO-FOCUS X-RAY CT SYSTEM AND DISCUSSIONS

The tested samples were placed on the sample table and scanned by cone beam geometry X-ray generator covering 35 mm in diameter and 35 mm high after the dynamic test. The source voltage and source current to accelerate the electrons were 130 kV and 120 μA, respectively. The gain calibration was conducted to reduce the ring- and beam hardening artifacts using pre-filtering the X-ray beam by passing it thorough 6mm of aluminum. 459 X-ray attenuation slice images were scanned and the vertical slice width was 0.068 mm. The fragments of the test Inada granite specimen were reconstructed for the X-ray CT scanning.

Figure 4 (a) shows the volume-rendering 3D reconstruction image for B1 test sample. The image set contains 1024×1024×650 voxels (voxel resolution is 7.6 μm). Figures 4 (b)-(d) show selected cross-sectional images of centre X-Y, X-Z and Y-X slices, respectively. Material constituents and pores are visible. The contrast in the images shows differences in the density of mineral; that is, the white portions indicate the places where high density minerals exist such as metallic minerals.

Figure 5 shows selected cross-sectional slice images of center XY for the tested samples. The cracks increase as impact velocity increase. The most of the cracks generate alongside the boundaries of the material constitutes and connect the pores. The image for B2 sample shows radial cracks connecting the out surface of the cylindrical sample.

Figure 6 selected cross-sectional slice images of center YZ for tested samples. The upper side and lower side correspond to the contact sides with the transmitted bar and incident bar, respectively. The density of the vertical cracks increased with increasing impact velocity during the testes. A number of cracks which are not connected each other are visible. At the impact velocity of 14m/s, spalls (parallel to the loading axis) occur near the out surface of the cylindrical sample. The most of vertical cracks generate along the boundaries of the material constitutes and connect the pores. At the impact velocity of 18m/s, cracks coalescence and these result in numerous fragments.

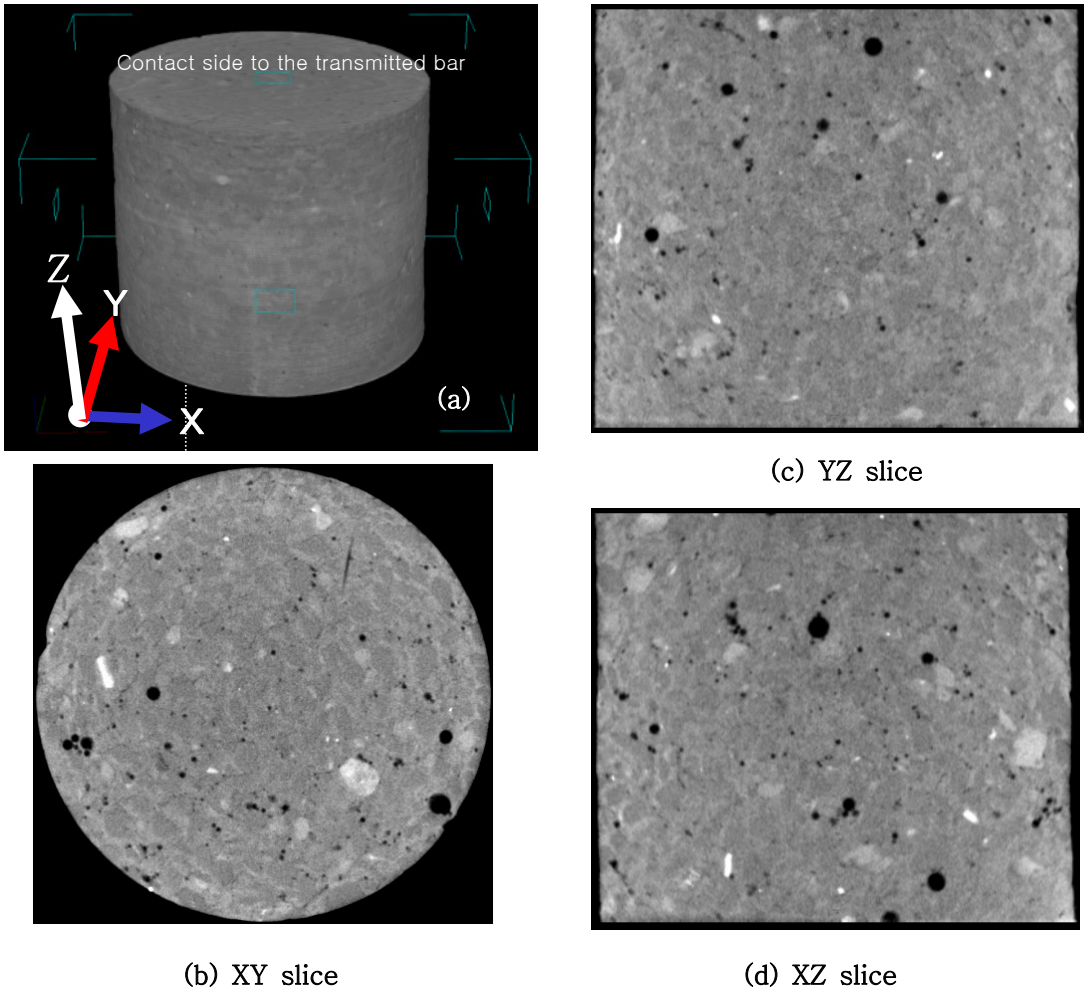


Fig. 4 3D structure of B1 test sample (a) Volume-rendering image from 459 X-ray attenuation images, (b) Cross-sectional image of centre XY slice, (c) Selected cross-sectional image of centre XZ slice, and (d) Selected cross-sectional image of centre YZ slice.

Figure 7 selected cross-sectional slice images of center YZ for tested samples. These images also show that the density of the vertical cracks increased with increasing impact velocity during the testes. Cracks caused by tensile cracks and wing cracks are visible at the samples subjected to the impact velocity exceeds 14m/s. The vertical crack which is indicated by the white ellipse is composed of tensile fractures connected by wing cracks. Numerous cracks that do not coalesce to form a single macro crack are visible. This study shows that micro X-ray CT system with a high spatial resolution is a useful tool for observing cracks and internal structure of the cement paste samples subject to dynamic loading.

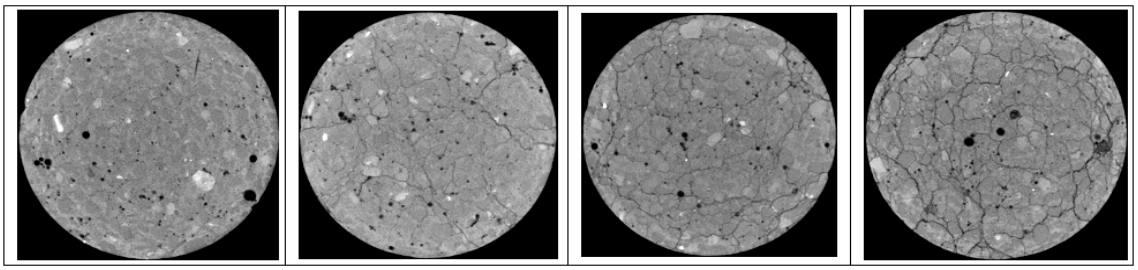

B1 B2 B3 B4

Fig. 5 Cross-sectional image of centre XY slice for the test samples

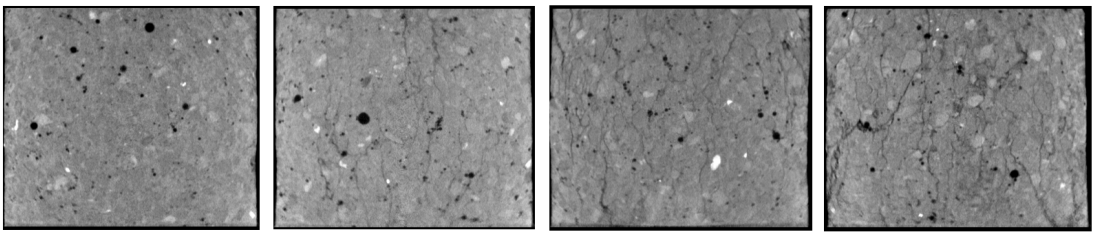

B1 B2 B3 B4

Fig. 6 Cross-sectional image of centre YZ slice for the test samples

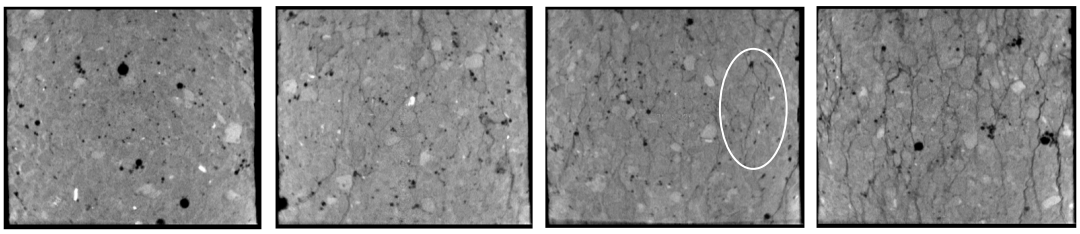

B1 B2 B3 B4

Fig. 7 Cross-sectional image of centre XZ slice for the test samples

## 5. CONCLUSIONS

This study employed a pulse shape technique into conventional SHPB to make dynamic loading-induced damage samples which have different damage levels. Apparent strain increased as impact velocity increased while the elastic wave velocity decreased. The cracks inside the tested samples were observed using micro focused X-ray CT. The cracks increase as impact velocity increase. The most of the cracks generate alongside the boundaries of the material constitutes and connect the pores. The density of

the vertical cracks increased with increasing impact velocity during the testes. A number of cracks which are not connected each other are visible. At the impact velocity of 14m/s, spalls occur near the out surface of the cylindrical sample. The most of vertical cracks generate alongside the boundaries of the material constitutes and are connecting the pores. At the impact velocity of 18m/s, cracks coalescence and these result in numerous fragments. Cracks caused by tensile cracks and wing cracks are visible at the samples subjected to the impact velocity exceeds 14m/s. Numerous cracks that do not coalesce to form a single macro crack are visible.

## ACKNOWLEDGEMENTS

The authors thank Ms. Mi-Jin Choi and Mr. Jung-Ryang Ahn for preparing the test samples and the tests. This research was supported by the Basic Research Project (Construction of deep underground research laboratory and core technology development) of the Korea Institute of Geoscience and Mineral Resources (KIGAM) funded by the Ministry of Science and Technology of Korea.

## REFERENCE

1. Kolsky H, “An Investigation of the mechanical properties of materials at very high rate of loading.” Proc. Roy. Soc. Lon. B. 62, 676-700, 1949

2. Gray G.T, “Classic split-Hopkinson pressure bar technique,” LAUR-99-2347. Los Alamos National Laboratory, 1999

3. Vinegar, H. J. 1986, X-ray CT and NMR imaging of rocks, J Pet Technol**,** Vol.38, No.3, 257-259

4. Lin C.L, Miller J.D, 1996, Cone beam X-ray microtomography for three-dimensional liberation analysis in the 21st century, Int. J. Miner. Process, 47, 61-73

5. Cho S.H, Yokota, Ogata Y, Kobota S, Kaneko K., 2005, Microscopic visualization in a granitic rock subjected to dynamic tensile loading by using microfocus X-ray CT, Science and Technology of Energetic Material Vol. 66, No.4 pp. 3348-3359

6. Nemat-Nasser S, Isaacs JB, Strttett JE, “Hopkinson techniques for dynamic recovery experiments” Pro. Roy.Soc.Lon. A 435 371-391, 1991

7. Cho SH, Mohanty B, Rajeev R, Xia K, Kaneko K, 2007, Fragmentation mechanism of rock in Split Hopkinson Pressure Bar (SHPB) test, 21st Canadian Congress of Applied Mechanics, Rye rson University, Toronto, Canada, June 3-7, pp. 607-608